Original Article
In vivo inflammation imaging using a CB$_2$R-targeted near infrared fluorescent probe

Shaojuan Zhang[1], Pin Shao[1], Xiaoxi Ling[1], Ling Yang[1,2], Weizhou Hou[3], Steve H Thorne[3], Wissam Beaino[1], Carolyn J Anderson[1,4,5], Ying Ding[6], Mingfeng Bai[1,4,5]

[1]Molecular Imaging Laboratory, Department of Radiology, University of Pittsburgh, Pittsburgh, PA 15219, USA; [2]Department of Cellular and Genetic Medicine, School of Basic Medical Sciences, Fudan University, Shanghai, 200032, China; [3]Division of Surgical Oncology and Department of Immunology, University of Pittsburgh Cancer Institute, Pittsburgh, PA 15213, USA; [4]Department of Bioengineering, University of Pittsburgh, Pittsburgh, PA 15261, USA; [5]University of Pittsburgh Cancer Institute, Pittsburgh, PA 15232, USA; [6]Department of Biostatistics, University of Pittsburgh, Pittsburgh, PA 15261, USA

Abstract: Chronic inflammation is considered as a critical cause of a host of disorders, such as cancer, rheumatoid arthritis, atherosclerosis, and neurodegenerative diseases, although the exact mechanism is yet to be explored. Imaging tools that can specifically target inflammation are therefore important to help reveal the role of inflammation in disease progression, and allows for developing new therapeutic strategies to ultimately improve patient care. The purpose of this study was to develop a new *in vivo* inflammation imaging approach by targeting the cannabinoid receptor type 2 (CB$_2$R), an emerging inflammation biomarker, using a unique near infrared (NIR) fluorescent probe. Herein, we report the first *in vivo* CB$_2$R-targeted NIR inflammation imaging study using a synthetic fluorescent probe developed in our laboratory, NIR760-mbc94. *In vitro* binding assay and fluorescence microscopy study indicate NIR760-mbc94 specifically binds towards CB$_2$R in mouse RAW264.7 macrophage cells. Furthermore, *in vivo* imaging was performed using a Complete Freund's Adjuvant (CFA)-induced inflammation mouse model. NIR760-mbc94 successfully identified inflamed tissues and the probe uptake was blocked by a CB$_2$R ligand, SR144528. Additionally, immunofluorescence staining in cryosectioned tissues validated the NIR760-mbc94 uptake in inflamed tissues. In conclusion, this study reports the first *in vivo* CB$_2$R-targeted inflammation imaging using an NIR fluorescent probe. Specific targeting of NIR760-mbc94 has been demonstrated in macrophage cells, as well as a CFA-induced inflammation mouse model. The combined evidence indicates that NIR760-mbc94 is a promising inflammation imaging probe. Moreover, *in vivo* CB$_2$R-targeted fluorescence imaging may have potential in the study of inflammation-related diseases.

Keywords: Inflammation, cannabinoid receptor, CB$_2$, fluorescent probe, optical imaging, near infrared

Introduction

Inflammation is a response from host defense to stimuli that initiate the repair of damaged tissues and the removal of harmful stimuli. While acute inflammation typically results in healing, chronic inflammation is associated with many types of diseases, such as cancer, arthritis, atherosclerosis, autoimmune diseases, stroke, and neurodegenerative diseases [1, 2]. Moreover, inflammation has been found to promote and aggravate the disease conditions [3]. Unfortunately, the mechanism of systemic chronic inflammation is still poorly understood, and therefore imaging tools that can specifically target inflammation are needed to help uncover the role of inflammation in disease progression and provide insights into developing new therapeutic strategies to ultimately improve patient care.

Near infrared (NIR) fluorescence imaging is emerging as an attractive imaging technique for *in vivo* inflammation imaging in real time. Although a few magnetic resonance imaging (MRI) [4] and positron emission tomography (PET) [5] probes for inflammation imaging have been developed, fluorescence imaging has the advantages of high sensitivity and resolution, as well as low instrument cost. The main limita-

tion of optical imaging (i.e., limited tissue penetration caused by tissue absorption and scattering) can be partially resolved by adopting NIR light, which improves tissue penetration and minimizes tissue autofluorescence [6]. As such, NIR fluorescence imaging has been widely used in preclinical and clinical imaging studies [7, 8]. Typically, inflammation-targeted NIR fluorescence imaging is achieved with fluorescent nanoparticles, which can be internalized by macrophages. These nanoparticles either have intrinsic fluorescence (*e.g.*, quantum dots [9]) or incorporate fluorescent dyes into the nanostructure (*e.g.* perfluorocarbon nanoemulsions loaded with NIR dyes in the oil layer [10, 11]) or onto the nanoparticle surface through bioconjugation (*e.g.* VT680 dye attached to the surface of dextran-coated iron oxide nanoparticles [12]). Although macrophages are effective in taking up nanoparticles, other than a few "smart" probes that can be activated by certain proteases (*e.g.* matrix metalloproteinases and cysteinyl cathepsins) produced by macrophages [13-15], most of these nanoparticles have limited selectivity due to the lack of effective targeting strategies. Recently, a couple of small NIR fluorescent dyes identified from screening have been shown to preferably bind to macrophages; however, the targeting mechanism remains unclear [16, 17], leading to difficulties in thorough data interpretation and probe optimization.

In an effort to develop novel inflammation-targeted NIR fluorescent probes that can target alternative inflammation biomarkers and potentially provide new insights on the role of inflammation in disease progression, here we report the first *in vivo* cannabinoid CB2 receptors (CB$_2$R)-targeted NIR inflammation imaging study using a synthetic fluorescent probe developed in our laboratory, NIR760-mbc94. Due to the important regulatory role, CB$_2$R is emerging as an attractive biomarker for inflammation research. Under homeostatic conditions, CB$_2$R is predominantly a peripheral receptor abundantly expressed by immune cells [18, 19], although limited expression in brain was also reported [20]. Accumulated evidences indicate that CB$_2$R agonists exhibit promising therapeutic value for treating inflammation [21]. Therefore, CB$_2$R-targeted imaging tools have promise in imaging inflammation and exploring the therapeutic value of CB$_2$R. Both *in vitro* binding assay and fluorescence microscopy studies

suggest that NIR760-mbc94 specifically labels mouse macrophage RAW264.7 cells. In a Complete Freund's Adjuvant (CFA)-induced inflammation mouse model, NIR760-mbc94 successfully identified inflamed tissues and the probe uptake was blocked by a CB$_2$R ligand, SR144528. Additionally, NIR760-mbc94 uptake by macrophages was visualized in cryosectioned inflamed tissues.

Materials and methods

Cell culture

RAW264.7 mouse macrophage cells were used for *in vitro* studies (a gift from Dr. Jelena Janjic at Duquesne University). RAW264.7 cells were activated by treating with 200 ng/mL lipopolysaccharides (LPS, Sigma-Aldrich, St. Louis, MO) for 24 h at 37°C. Mouse Delay Brain Tumor-Wild Type (DBT-WT, non CB$_2$R expressing) cells were used as the negative control. RAW264.7 cells were cultured in Dulbecco's Modified Eagle's Medium (DMEM, Sigma-Aldrich, St. Louis, MO) supplemented with 10% Fetal Bovine Serum (FBS), 10 mM HEPES (Life Technology, Carlsbad, CA), 1 × Penicillin-Streptomycin-Glutamine (Life Technology, Carlsbad, CA). DBT-WT cells were cultured in DMEM supplemented with 10% FBS and 1 × Penicillin-Streptomycin-Glutamine. Cells were cultured at 37°C in a humidified incubator in an atmosphere of 5% CO$_2$.

Reverse transcription polymerase chain reaction (RT-PCR) and western blot

To determine CB$_2$R mRNA and protein expression level in RAW264.7, LPS-treated RAW264.7 and DBT-WT cells, RT-PCR and western blot were conducted as previously reported [22]. For RT-PCR, The sequences used for mouse CB$_2$R primers were 5'-tcctatcatttacgccctgc-3' (sense) and 5'-ggctcctaggtggttttcacatcagcctc-3' (antisense). GAPDH (primer sequences: 5'-tgaacgggaagctcactggcat-3' (sense) and 5'-tgcctgcttcaccaccttcttg-3' (antisense)) was used for template normalization. Amplifications were run using Platinum Taq DNA polymerase (Invitrogen, Carlsbad, CA) and consisted of 33 cycles of 30 s at 94°C, 30 s at 55°C, and 30 s at 72°C. For western blot, anti-CB$_2$R monoclonal antibody (Sigma-Aldrich, St. Louis, MO) was used as primary antibody. Anti-mouse IgG, HRP-linked antibody (Cell Signaling Technology,

Danvers, MA) was used as secondary antibody.

In vitro binding assay

We used RAW264.7 and DBT-WT cells for *in vitro* binding assay. 1 × 10^4 cells (per well) were seeded onto 96-well black polystyrene optical bottom plates (Thermo Scientific, Pittsburgh, PA). Cells were incubated at 37°C for 48 h prior to treatment of fluorescent probes. For LPS-treated RAW264.7 cells, RAW264.7 cells were seeded onto 96-well optical black plates and incubated at 37°C for 24 h and subsequently treated with 200 ng/mL of LPS for an additional 24 h at 37°C. Cells were treated with 1.0 µM of NIR760-mbc94 or NIR760 at 37°C for 30 min, with or without pretreatment of 2.0 µM blocking agent SR144528 at 37°C for 30 min. A Synergy™ H4 Hybrid Multi-Mode Microplate Reader (BioTek, Winooski, VT) was used to read fluorescence at 740/790 nm (excitation/emission). After the initial reading, cells were rinsed with cell culture medium twice and the fluorescence emission was measured again. The fluorescence emission spectra recorded were normalized by dividing each point by the initial reading and then corrected with cell number (with data expressed in terms of relative fluorescence units, RFU). Each data point represents the mean ± SEM based on triplicate samples. The cell numbers were obtained as follow: cells were fixed in 4% paraformaldehyde in PBS (Affymetrix, Santa Clara, CA) for 10 min at 25°C, permeabilized with 0.1% Triton X-100 in PBS (Sigma-Aldrich, St. Louis, MO) for 5 min at 25°C and rinsed twice with PBS. Then, DRAQ-5 (1:2500) was added for 5 min at 25°C and rinsed twice with PBS. Fluorescence at 650/690 nm (excitation/emission) was recorded for cell number quantification.

Cell fluorescence imaging

RAW264.7 and DBT-WT cells (1 × 10^4 cells) were seeded into 8-well chamber slide (Thermo Scientific, Pittsburgh, PA) incubated at 37°C for 48 h. For LPS-treated RAW264.7 cells, RAW-264.7 cells were seeded into 8-well chamber slide and incubated at 37°C for 24 h and subsequently treated with 200 ng/mL of LPS for an additional 24 h at 37°C. Cells were treated with 1.0 µM of NIR760-mbc94 or NIR760 at 37°C for 30 min, with or without pretreatment of 2.0 µM blocking agent SR144528 at 37°C for 30
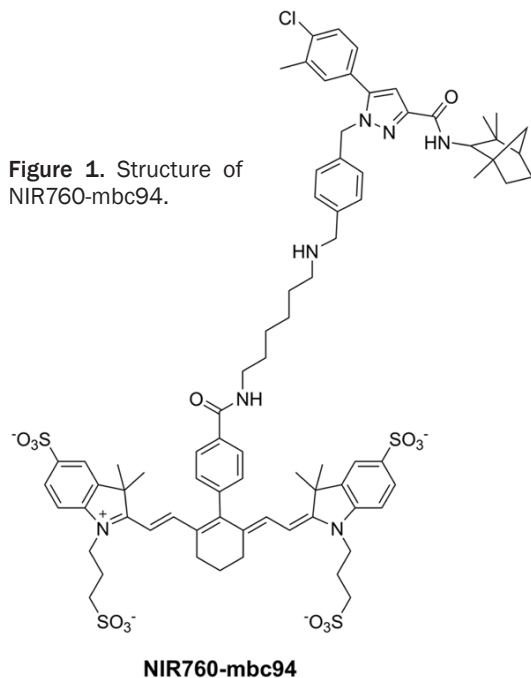
min. After the incubation, cells were washed three times with cell culture medium to remove the unbound probe, and fixed with 4% paraformaldehyde in PBS for 20 min at 25°C. Cells were then permeabilized with 0.1% Triton X-100 in PBS. The cell nucleus was stained with 10 µg/mL DAPI (Life Technologies, Carlsbad, CA) for 15 min at 25°C and rinsed three times with PBS. Cells were mounted with ProLong® Gold antifade reagent (Life Technologies, Carlsbad, CA) and then imaged using the Zeiss Axio Observer fluorescence microscope equipped with the ApoTome 2 imaging system (Carl Zeiss Microimaging Gmbh, Jena, Germany). NIR probes images were captured with a NIR camera with an indocyanine green (ICG) filter set (excitation/emission: 750-800/820-875 nm). Nuclear images were obtained with a DAPI filter set (excitation/emission: 335-383/420-470 nm). Differential interference contrast (DIC) images were obtained through Trans light DIC. All the fluorescence images are captured using the same parameters (*i.e.* exposure time, gain, etc.). All images were processed using Zen 2011 (Carl Zeiss Microimaging Gmbh, Jena, Germany) at the same fluorescence intensity scale.

In vivo inflammation imaging

All animal experiments were performed in accordance with the guidelines for the Care and Use of Laboratory Animals of the Medical Research Council of University of Pittsburgh. CFA-induced inflammation model was developed in the left paw of 6-8 week old female nude mice as described below. Nine mice were anesthetized with a 2.5% isoflurane/oxygen gas mixture. 50 µL of CFA (MP Biomedicals, LLC, Solon, OH) and PBS mixture (CFA : PBS = 1:1) was injected into the footpad of left paw [23]. The untreated right paw was used as the negative control. At 12 h post-injection, inflammation was well stimulated in the left paw. The mice were assigned into three groups for different i.v. injection with imaging agents in 100 µL saline via tail vein as follow: (1) three mice with 10 nmol of NIR760-mbc94; (2) three mice with 100 nmol of SR144528 followed by 10 nmol NIR760-mbc94 after 1 h; (3) three mice with 10 nmol of NIR760.

Optical imaging was performed with a charge-coupled device camera–based bioluminescence imaging system IVIS Lumina XR (PerkinElmer, Waltham, MA) using the following

Figure 1. Structure of NIR760-mbc94.

NIR760-mbc94

Figure 2. CB$_2$R expression in RAW264.7 and DBT-WT cells. A. CB$_2$R (55 kDa) and β-actin (42 kDa) protein expression was determined by western blot. B. CB$_2$R mRNA (165 bp) and GAPDH (124 bp) expression was determined by RT-PCR.
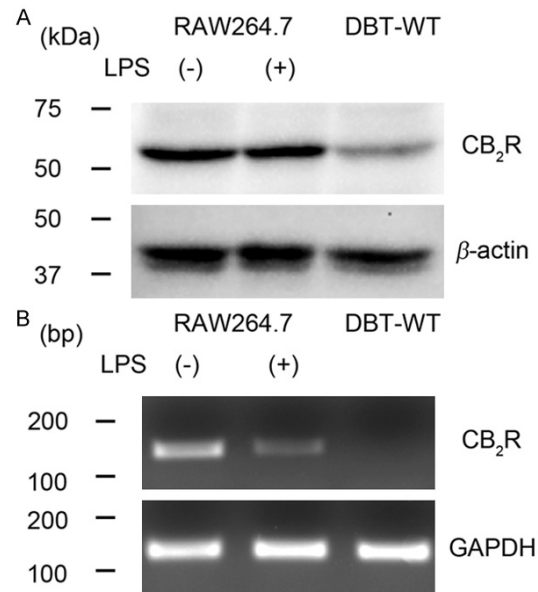
parameters: excitation filter, 745 nm; emission filter, 800 nm; exposure time, 1 sec; binning, small; field of view, 12; f/stop, 2; open filter. The images were captured at pre-injection and 0.5, 1, 4, 8, 12, 24, 36, and 48 h post-injection. Signal was displayed as Radiant Efficiency ([photons/sec/cm^2/sr]/[μW/cm^2]). Images were analyzed by using Living Image 4.4 software (Caliper Life Sciences, Hopkinton, MA). Region-of-interest (ROI) on the affected left paw (INF) and control right paw (Non-INF) were drawn. The contrast enhancement profiles of NIR760-mbc94 uptake in inflamed area were obtained by dividing INF by Non-INF.

Ex vivo imaging

After the last time point (48 h post-injection) of *in vivo* imaging, all mice were euthanized. The paws and selected tissues and organs (blood, heart, lung, liver, spleen, pancreas, kidneys, muscle from right leg, and brain) were excised and imaged under IVIS Lumina XR system. The fluorescent intensity of the NIR760-mbc94 and NIR760 in the corresponding mice groups was evaluated by drawing ROI along the excised tissues and organs. The quantitative fluorescent intensity contrast profiles were obtained by dividing target by control paw.

To determine the tissue or organ uptake of NIR760-mbc94 at earlier post-injection time

point, 10 nmol of NIR760-mbc94 was i.v. injected into two nude mice. The mice were euthanized 30 min and 1 h post-injection, respectively. Major tissues and organs (blood, heart, lung, liver, spleen, pancreas, kidneys, muscle from right leg, and brain) were excised and imaged under IVIS Lumina XR system. The images were processed similarly as above.

Immunofluorescence staining on frozen paw sections

Paws of mice were excised and divided into four groups for histological investigation as follow: (1) INF from mice injected with NIR760-mbc94; (2) Non-INF from mice injected with NIR760-mbc94; (3) INF from mice injected with NIR760-mbc94 with pretreatment of SR144528; (4) INF from mice injected with NIR760. All paw samples were flash frozen in Tissue-Tek O.C.T. compound mounting medium (Sakura Finetek, Torrance, CA), and cryostat-sectioned (10 μm) using a Microm HM 500 DM Cryostat (MICROM International GmbH, Walldorf, Germany). Tissue slices were fixed in acetone for 10 min. The slices were then immunostained with anti-CD-68 anitbody (Bio-Rad AbD Serotec, Oxford, UK) for 1 h at 25°C (1:300 in 0.2% BSA, 0.05% Tween20 in PBS) as primary antibody, followed by anti-rat Alexa Fluor 488 (Invitrogen, Grand
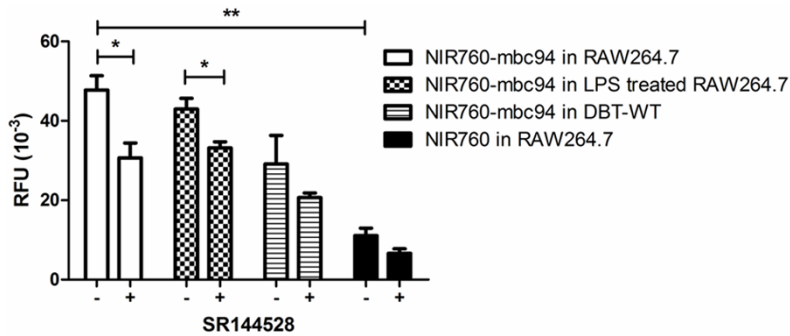
Figure 3. *In vitro* binding assay. Cells were treated with NIR760-mbc94, with or without pretreatment of SR144528 (blocking agent). NIR760 without CB$_2$R-targeted moiety was used as a control. After removal of the unbound probes, fluorescence intensity at 790 nm was measured and represented as RFU. Each data point represents the mean ± SEM based on triplicate samples (*$p < 0.05$; **$p < 0.01$).

Island, NY) for 1 h at 25°C (1:500 in 0.2% BSA, 0.05% Tween20 in PBS) as fluorochrome-conjugated secondary antibody. The slices were stained with 10 μg/mL DAPI for 15 min at 25°C. Zeiss Axio Observer fluorescent microscope was used to capture fluorescence images. NIR760-mbc94 or NIR760 was directly visualized with an ICG filter (excitation/emission: 750-800/820-875 nm). Macrophage cells were visualized with a green fluorescent protein (GFP) filter (excitation/emission: 450-490/500-550 nm). Nuclear images were visualized with a DAPI filter (excitation/emission: 335-383/420-470 nm).

Data processing and statistics

All of the data given in this study are the mean ± SEM (standard error of the mean) of 3 independent measurements. For *in vitro* binding study and *ex vivo* imaging study, statistical analyses were performed using the one-way ANOVA method, with *p* values < 0.05 considered statistically significant. For *in vivo* imaging studies, statistical analyses were performed using the repeated measures ANOVA (all data from 0-48 h were utilized), with *p* values < 0.05 considered statistically significant. The analyses were performed using SAS 9.4 (SAS Institute Inc., Cary, NC).

Results

*CB$_2$R-targeted NIR fluorescent probe specifically labels macrophages in vitro*

The CB$_2$R-targeted NIR fluorescent probe, NIR760-mbc94 (**Figure 1**), consists of an NIR

fluorescent dye, NIR760, and a CB$_2$R-targeting molecule, mbc94. NIR760-mbc-94 and NIR760 were prepared as we previously reported [22]. NIR760-mbc94 exhibits intense NIR absorption and emission peaked at 766 nm and 785 nm in water respectively [22].

To study target-specific uptake of NIR760-mbc94 *in vitro*, we first characterized the CB$_2$R protein and mRNA expression level in regular RAW264.7 (mouse macrophages), LPS-treated RAW-264.7 (activated macrophages) and CB$_2$R-negative wild type delayed brain tumor (DBT-WT) cells. As shown in **Figure 2**, positive CB$_2$R protein and mRNA expression was observed in both activated and regular RAW264.7 cells, and negligible level was observed in DBT-WT cells. In addition, treatment of LPS greatly decreased CB$_2$R mRNA expression in RAW264.7 cells (**Figure 2B**). Next, we carried out cellular binding assay to evaluate the specific binding of NIR760-mbc94 to CB$_2$R expressed by macrophages using a microplate reader (**Figure 3**). Four-fold higher fluorescent signal (RFU (10^{-3}): 47.8 ± 3.6 vs 11.1 ± 1.9, **$p < 0.01$, respectively) was observed when the RAW264.7 cells were treated with NIR760-mbc94 than with non-targeted NIR760 (free dye control). In addition, SR144528, which is a widely used CB$_2$R inverse agonist and was used as the blocking agent here, reduced the fluorescence signal of NIR760-mbc94 in regular RAW264.7 cells by 36% (RFU (10^{-3}): 30.7 ± 3.8 vs 47.8 ± 3.6, *$p < 0.05$, respectively) and activated RAW264.7 cells by 23% (RFU (10^{-3}): 33.2 ± 1.6 vs 43.0 ± 2.7, *$p < 0.05$, respectively). As expected, no significant blocking effect was observed in CB$_2$R-negative DBT-WT cells (RFU (10^{-3}): 20.7 ± 1.1 vs 29.7 ± 7.2, $p > 0.05$, respectively). These data indicate the specific binding of the NIR760-mbc94 probe to the target receptor.

NIR fluorescence microscopy was then conducted to visualize the uptake of NIR760-mbc94 in RAW264.7, LPS-treated RAW264.7 and DBT-WT cells. As shown in **Figure 4A**, NIR760-mbc94 was predominantly localized in cytoplasm of RAW264.7 and LPS-treated
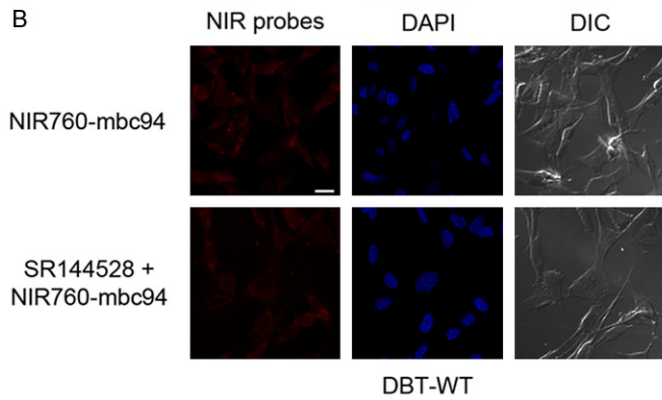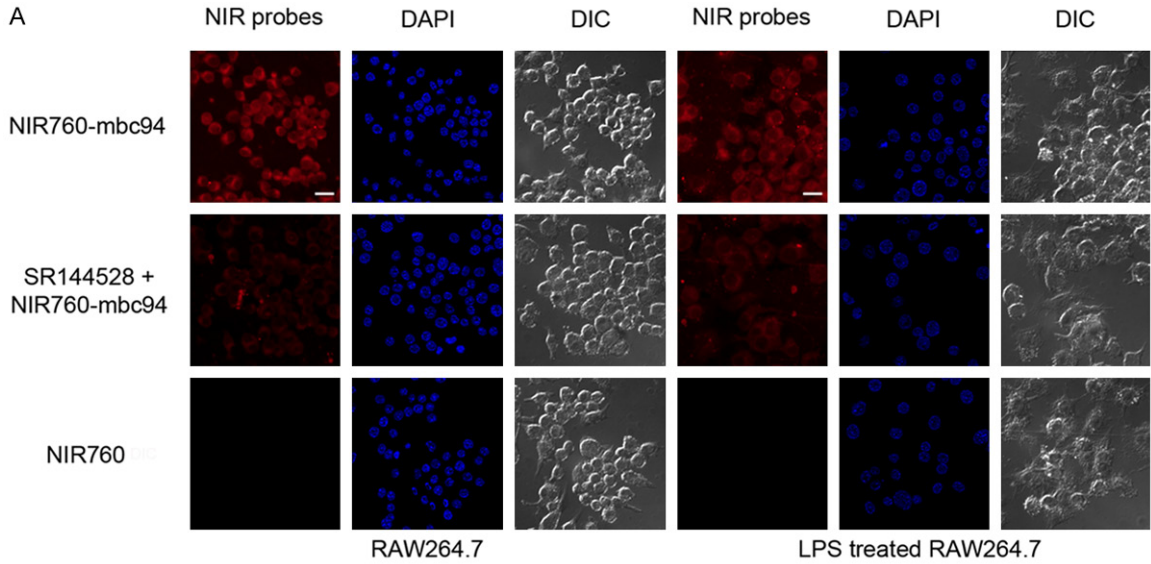
Figure 4. Cellular uptake of NIR760-mbc94 visualized by fluorescence microscopy. A. RAW-264.7 and LPS-treated RAW264.7 cells were treated with NIR760-mbc94, with or without pretreatment of blocking agent SR144528. Non-targeted NIR760 was used as the free dye control. B. DBT-WT cells were treated with NIR760-mbc94, with or without pretreatment of blocking agent SR144528. After removal of the unbound probes, cells were imaged under fluorescence microscope. NIR760-mbc94 or NIR760 staining was shown under ICG filter. Nuclei were stained with DAPI and shown under DAPI filter. Scale bar = 20 μm.
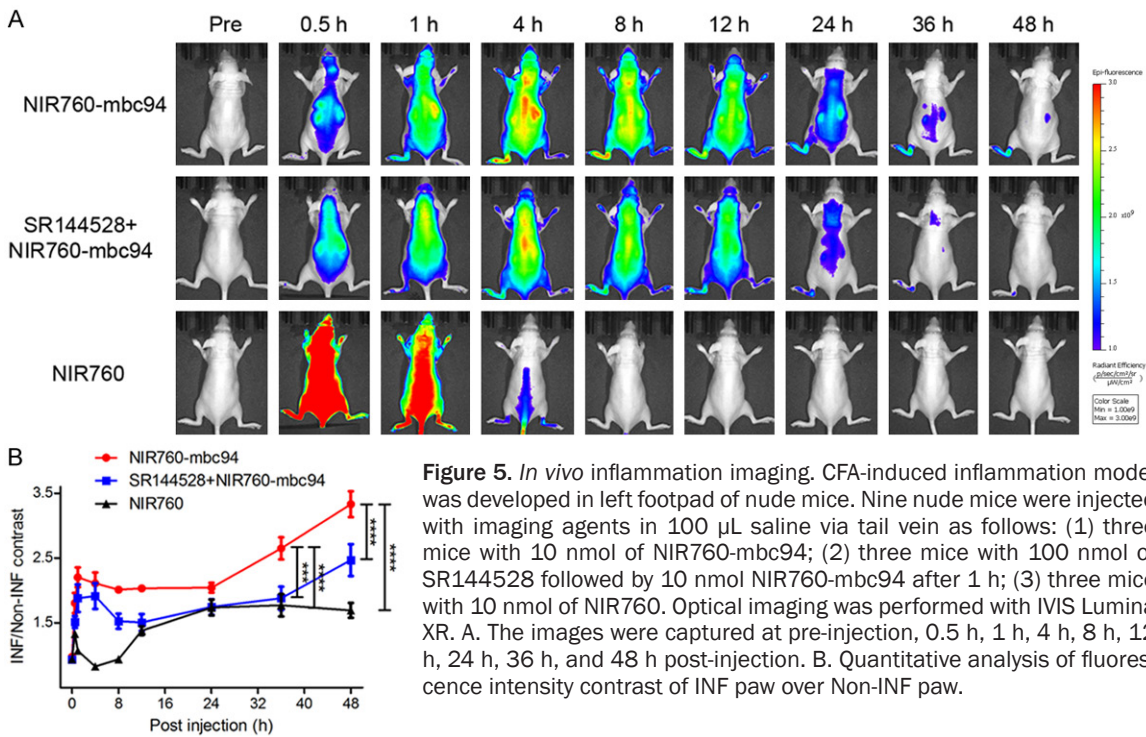
Figure 5. *In vivo* inflammation imaging. CFA-induced inflammation model was developed in left footpad of nude mice. Nine nude mice were injected with imaging agents in 100 μL saline via tail vein as follows: (1) three mice with 10 nmol of NIR760-mbc94; (2) three mice with 100 nmol of SR144528 followed by 10 nmol NIR760-mbc94 after 1 h; (3) three mice with 10 nmol of NIR760. Optical imaging was performed with IVIS Lumina XR. A. The images were captured at pre-injection, 0.5 h, 1 h, 4 h, 8 h, 12 h, 24 h, 36 h, and 48 h post-injection. B. Quantitative analysis of fluorescence intensity contrast of INF paw over Non-INF paw.
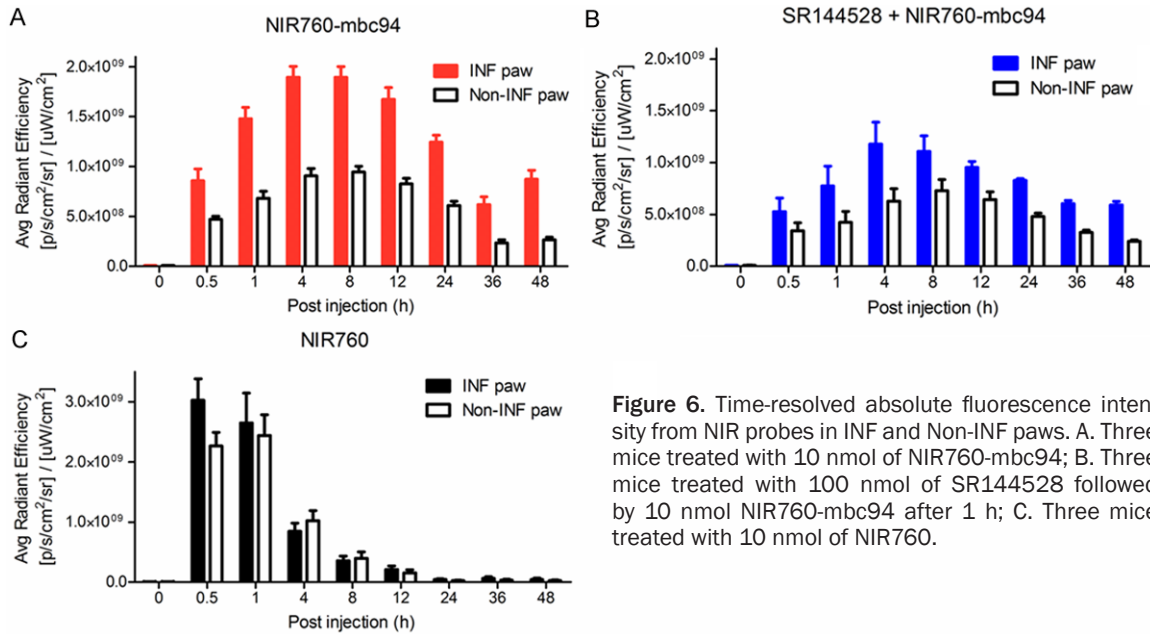
Figure 6. Time-resolved absolute fluorescence intensity from NIR probes in INF and Non-INF paws. A. Three mice treated with 10 nmol of NIR760-mbc94; B. Three mice treated with 100 nmol of SR144528 followed by 10 nmol NIR760-mbc94 after 1 h; C. Three mice treated with 10 nmol of NIR760.

RAW264.7 cells, whereas non-targeted NIR760 failed to show significant fluorescence signal. In addition, SR144528 dramatically reduced the uptake of NIR760-mbc94 in regular and activated RAW264.7 cells. In contrast, DBT-WT cells showed lower uptake of NIR760-mbc94 as compared to CB$_2$R-positive cells (**Figure 4B**). These data provided further evidence on the specific binding of NIR760-mbc94 to CB$_2$R.
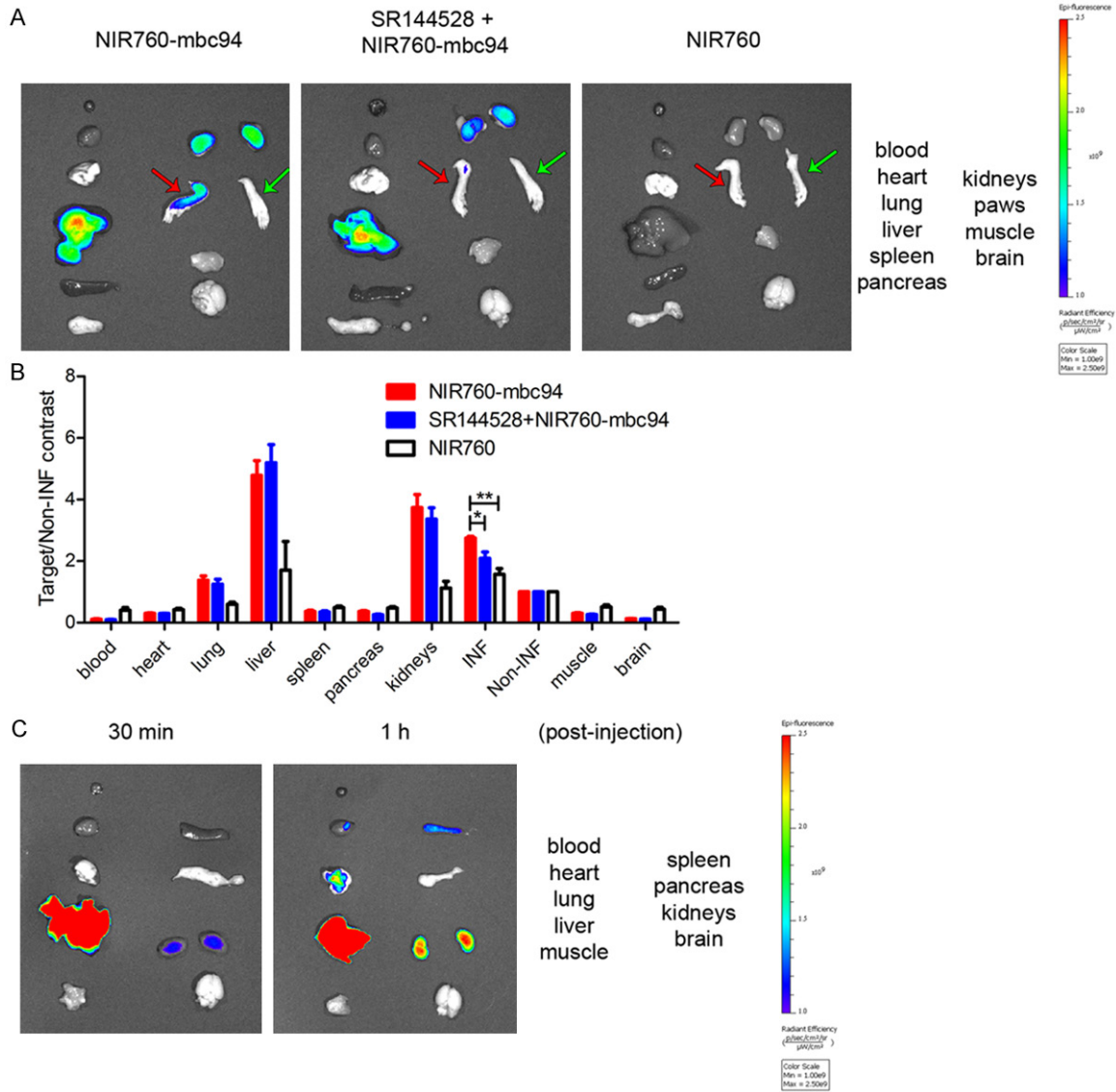
In vivo inflammation imaging

To explore the potential of NIR760-mbc94 for imaging inflammation *in vivo*, we used the CFA-induced inflammation mouse model. After the CFA/PBS mixture was topically injected into the left footpad of mice, classical signs of inflammation, such as redness and swelling, were observed in the affected area at 12 h post injection. A total of nine mice were divided into three groups (n = 3 for each group), received i.v. injection of fluorescent agents as shown below, and imaged: (1) three mice treated with 10 nmol of NIR760-mbc94; (2) three mice treated with 100 nmol of SR144528 followed by 10 nmol NIR760-mbc94 after 1 h; and (3) three mice treated with 10 nmol of non-targeting NIR-760. One representative mouse from each group was shown and all images are fluorescence images overlaid on the corresponding white light images (**Figure 5A**). Upon injection, NIR760-mbc94 dispersed rapidly in mice during the first 12 h and then underwent a delayed clearance after 24 h. Significantly higher uptake of NIR760-mbc94 was observed in the inflamed (INF) paw vs the non-inflamed paw (Non-INF) at all the post-injection time points. To quantify the imaging outcome (**Figure 5B**), the fluorescence signal in INF was divided by that in Non-INF to calculate the image contrast (INF/Non-INF), which gradually increased over the time course (ranging from 1.8 ± 0.2 at 30 min post-injection to 3.3 ± 0.2 at 48 h post-injection). The blocking agent, SR144528, significantly reduced the uptake of NIR760-mbc94 in the INF, with imaging contrast of 1.9 ± 0.2 vs 2.7 ± 0.2 (30% blocking effect, ***$p < 0.001$) at 36 h and 2.5 ± 0.2 vs 3.3 ± 0.2 (24% blocking effect, ****$p < 0.0001$) at 48 h post-injection. Additionally, the absolute fluorescence intensity in INF and Non-INF paw was compared to demonstrate that the background signals between the two groups are in similar level (**Figure 6A** and **6B**). Non-targeting NIR760 exhibited rapid distribution within 4 h post-injection followed by quick tissue clearance (**Figures 5B** and **6C**). The imaging contrast (INF/Non-INF) of NIR760 injected mice was significantly lower than that of NIR760-mbc94 injected mice, with the INF/Non-INF ratio of 1.8 ± 0.2 vs 2.7 ± 0.2 (****$p < 0.0001$) at 36 h and 1.7 ± 0.1 vs 3.3 ± 0.2 (****$p < 0.0001$) at 48 h post-injection. These data indicate that NIR-760-mbc94 specifically labeled CB$_2$R-expressing inflamed tissues *in vivo*.

Figure 7. *Ex vivo* inflammation imaging. A. *Ex vivo* imaging of tissues and organs after 48 h post injection of probes. The red arrow points to INF paw, and the green arrow points to the Non-INF paw. B. Quantitative analysis of fluorescence intensity contrast of tissues and organs over Non-INF paw. C. *Ex vivo* study on normal nude mice at 30 min and 1 h post i.v. injection of NIR760-mbc94.

Ex vivo inflammation imaging

To study the bio-distribution and further validate the *in vivo* binding specificity of NIR760-mbc94, all mice were euthanized after the last imaging time point. The paws and selected tissues and organs (blood, heart, lung, liver, spleen, pancreas, kidneys, muscle from right leg, and brain) were excised and imaged (**Figure 7A**). Similar to the *in vivo* imaging results, for mice injected with NIR760-mbc94, the INF showed higher fluorescence signal than the Non-INF (INF/Non-INF contrast = 2.8 ± 0.1). When

blocked by SR144528, the INF/Non-INF contrast significantly decreased (2.1 ± 0.2 vs 2.8 ± 0.1, *p < 0.05). In addition, mice injected with non-targeting NIR760 showed significantly lower INF/Non-INF contrast than the NIR760-mbc94 treatment group (1.6 ± 0.2 vs 2.8 ± 0.1, **p < 0.01, respectively). Other than the inflamed paws, liver and kidneys also exhibited high uptake of NIR760-mbc94, however, no blocking effect was observed in these organs (**Figure 7B**). Notably, limited amount of fluorescent intensity was observed from the spleen, which is known for high CB$_2$R expressing [18],
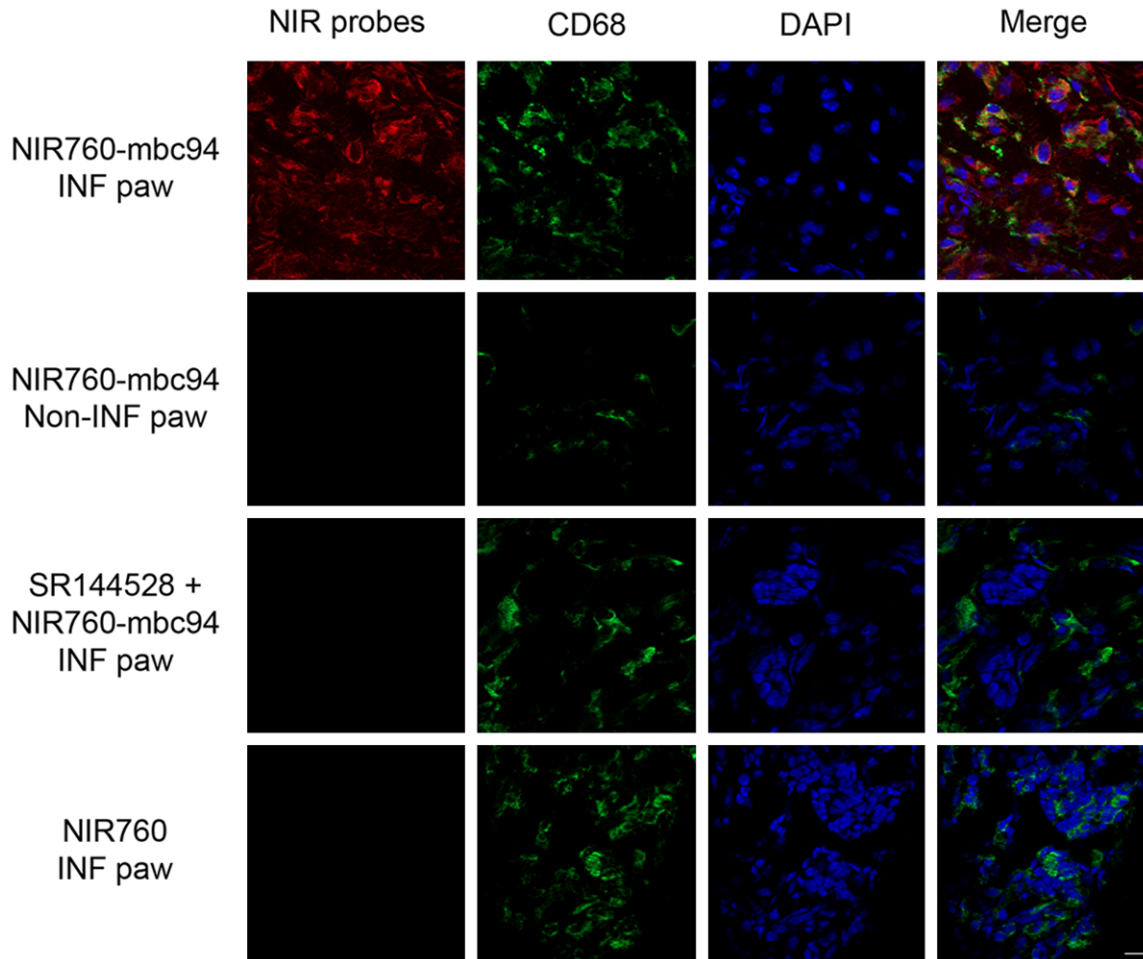
Figure 8. Immunofluorescence staining on frozen paw sections. Cryosection of paw samples were used for histological investigation. There are four groups of tissue slices: (1) INF from mice injected with NIR760-mbc94; (2) Non-INF from mice injected with NIR760-mbc94; (3) INF from mice injected with SR144528 followed by NIR760-mbc94; (4) INF from mice injected with NIR760. Slice images were obtained from fluorescent microscope. NIR760-mbc94 or NIR760 staining was shown under ICG filter. Macrophage cells were immunofluroescent stained with anti-CD68 staining and shown under GFP filter. Nuclear were stained with DAPI and shown under DAPI filter. Scale bar = 10 μm.

after 48 h post injection of the NIR probe. It is possible NIR760-mbc94 uptake in spleen has been cleared out at such a late time point. To study NIR760-mbc94 uptake at early time points, a preliminary biodistribution study at 30 min and 1 h post injection of the probe was conducted and significant spleen uptake of the probe at 1 h time point was observed (**Figure 7C**). These data provide further evidence on the specific uptake of NIR760-mbc94 by the CB$_2$R-expressing inflamed tissues.

Immunofluorescence staining on frozen paw sections

Having determined the specificity of NIR760-mbc94 for inflamed tissues *in vivo* and *ex vivo*,

we further characterized the binding profiles of NIR760-mbc94 at the tissue level. **Figure 8** shows the histological characterization results using frozen paw sectioning samples from the mice imaged *in vivo*. NIR fluorescence images (**Figure 8**, red, labeling NIR760-mbc94 or NIR-760) were collected using an ICG filter set and compared with fluorescence images (**Figure 8**, green, labelling macrophages) that correlate with a macrophage marker, CD68. As expected, strong NIR fluorescence signal was only identified in INF tissues from mice injected with NIR760-mbc94, whereas much lower fluorescence signal was detected in Non-INF tissues from NIR760-mbc94 injected mice, INF tissues from blocking agent injected mice (SR144528 + NIR760-mbc94) or non-targeted NIR760

injected mice. Importantly, for NIR760-mbc94 injected mice, fluorescence from CD68 largely colocalized with that from NIR760-mbc94 in INF tissues, suggesting the effectiveness of NIR760-mbc94 in labeling macrophages. It appears that NIR760-mbc94 also labeled additional cells as the NIR fluorescence covered larger area than the green fluorescence. This is not surprising because other types of CB$_2$R-expressing immune cells, such as neutrophils [24] and basophils [25], could have also been recruited by the inflamed tissues. Minimal green fluorescence was observed from Non-INF paw tissue samples, indicating low amount of macrophage cells. These findings indicate that, in histological level, NIR760-mbc94 accumulated in CFA-induced inflammation areas, where macrophage cells were abundant.

Discussion

The richness of inflammation involvement in various diseases has positioned inflammation as an attractive therapeutic target. The ability to noninvasively and specifically image inflammation would broaden our understanding on the role of inflammation in disease progression and mechanism of chronic inflammation, as well as facilitate the development of novel therapeutic techniques. As a major component of the mononuclear phagocyte system, macrophages play a critical role of initiation, maintenance and resolution of inflammation, and therefore has become a common target for inflammation imaging [26, 27]. The high endocytosis activity of macrophages has provided opportunities to image inflammation using nanomaterials, such as superparamagnetic iron oxide nanoparticles for MRI [28], ^{64}Cu-labeled nanoparticles for PET imaging [29], and fluorescent dye-labeled nanoparticles for optical imaging [30]. Although many of these nanoparticles have been shown to be effective in macrophage labeling, significant challenges still exist. For example, it is difficult to selectively label immune cell subsets (*e.g.* macrophages versus B cells) and target "bad" vs "good" macrophages. Additionally, relatively large nanoparticles typically experience prolonged circulation time, leading to poor imaging contrast [31]. We postulate that small molecule-based imaging probes with targeting functionalities would have promise in inflammation imaging due to the desired plasma circulation time, easily characterized structure and straightforward

targeting strategy (no concerns of endocytosis vs receptor targeting).

An advantage of targeting CB$_2$R for inflammation imaging is the potential of high imaging contrast. Under basal conditions, CB$_2$R has low expression throughout the organism, other than in tissues that contain B cells of the immune system [32]. Indeed, CB$_2$R expression is high only in spleen and lymph nodes, and low - or even undetectable - in brain, thyroid, retina, placenta, skeletal muscle, kidney, liver, adrenal gland, heart, prostate and ovary [33, 34]. However, as much as a 100-fold increase of CB$_2$R mRNA level documented during inflammation [35, 36]. Such high up-regulation of CB$_2$R provides opportunities for high contrast inflammation imaging.

The goal of this work was to develop a new *in vivo* NIR inflammation imaging approach by targeting CB$_2$R, which is an emerging biomarker of inflammation. Although a few CB$_2$R ligands have been radiolabeled and evaluated in neuroinflammation imaging, no *in vivo* CB$_2$R-targeted NIR fluorescence imaging of inflammation has been reported [37-39]. Using a unique CB$_2$R-targeted NIR fluorescence probe we recently reported [22], NIR760-mbc94 (**Figure 1**), we conducted NIR fluorescence imaging of inflammation *in vitro* and *in vivo*. CB$_2$R-expressing RAW264.7 cells were used for *in vitro* studies and CB$_2$R-negative DBT-WT cells were used as the control cells (**Figure 2**). Similar CB$_2$R protein expression level was characterized in LPS treated and regular RAW264.7 cells, but decreased level of CB$_2$R mRNA expression level was found in LPS treated RAW264.7 cells, which is consistent with recent reports [40]. As expected, negligible CB$_2$R protein and mRNA expression was characterized in DBT-WT cells. NIR760-mbc94 specifically binds to CB$_2$R in both LPS treated and untreated RAW264.7, but not in cells expressing low level of CB$_2$R, as evidenced by studies from a cell binding assay (**Figure 3**), and fluorescent microscopy (**Figure 4**). These results are similar to our previous cellular imaging studies using a CB$_2$R-transfected tumor cell line [22].

Building upon the findings from cellular imaging studies, we further evaluated the *in vivo* imaging potential of NIR760-mbc94 in a mouse inflammation model. Several agents have been reported to stimulate inflammation *in vivo*, including CFA, carrageenan, and LPS [16]. Here

we injected CFA to the left footpad of mice to stimulate inflammation. After injection of the fluorescent probe, higher NIR fluorescence signals in INF than in the Non-INF were observed at all time points indicating a regional-selective probe uptake. In contrast, such selectivity was not observed in mice injected with the non-targeting NIR760 (**Figures 5-7**). As such, NIR760-mbc94 may be applied as a potential fluorescent contrast agent for inflammation lesions detection. Moreover, CB$_2$R reverse agonist SR144528 successfully blocked uptake of NIR760-mbc94 in INF, which indicates NIR760-mbc94 labels inflamed areas through a CB$_2$R-specific binding. Immunostaining on frozen sectioned paw samples also validated the above findings (**Figure 8**). Strong fluorescence signals of NIR760-mbc94, the majority of which are co-localized with CD68-labeled macrophage cells, were observed in inflamed paw tissues. It is worth noting that, besides macrophages, additional areas were stained with NIR760-mbc94. This is possible as other types of inflamed cells also express CB$_2$R [33].

We also noted that the binding specificity of NIR760-mbc94 is relatively low. It is common in molecular CB$_2$R probes design that the binding property of the ligand is compromised upon conjugation with bulky fluorophore [41]. A key effort in our laboratory is to develop new CB$_2$R-targeting NIR fluorescent probes with improved binding specificity. Further work may involve applying these new probes in inflammation imaging studies.

Conclusion

This study reports the first *in vivo* CB$_2$R-targeted inflammation imaging using an NIR fluorescence probe. Specific targeting of NIR760-mbc94 has been demonstrated in macrophages, a CFA-induced inflammation mouse model and *ex vivo* inflamed tissues. The combined evidence indicates that NIR760-mbc94 is a promising inflammation imaging probe. As a new inflammation imaging approach, *in vivo* CB$_2$R-targeted fluorescence imaging may be helpful in the study of various diseases and shine light on the mechanism of disease progression involving immune cells.

Acknowledgements

Disclosure of conflict of interest

No potential conflicts of interest relevant to this article are reported.

Address correspondence to: Mingfeng Bai, Molecular Imaging Laboratory, Department of Radiology, University of Pittsburgh, Pittsburgh, PA 15219, USA; Department of Bioengineering, University of Pittsburgh, Pittsburgh, PA 15261, USA & University of Pittsburgh Cancer Institute, Pittsburgh, PA 15232, USA. Tel: 412-624-2565; Fax: 412-624-2598; E-mail: baim@upmc.edu

References

[1] Weiss U. Inflammation. Nature 2008; 454: 427.

[2] Laveti D, Kumar M, Hemalatha R, Sistla R, Naidu VG, Talla V, Verma V, Kaur N and Nagpal R. Anti-inflammatory treatments for chronic diseases: a review. Inflamm Allergy Drug Targets 2013; 12: 349-61.

[3] Krishnamoorthy S and Honn KV. Inflammation and disease progression. Cancer Metastasis Rev 2006; 25: 481-91.

[4] Kircher MF, Gambhir SS and Grimm J. Noninvasive cell-tracking methods. Nat Rev Clin Oncol 2011; 8: 677-88.

[5] Wu C, Li F, Niu G and Chen X. PET imaging of inflammation biomarkers. Theranostics 2013; 3: 448-66.

[6] Frangioni JV. In vivo near-infrared fluorescence imaging. Curr Opin Chem Biol 2003; 7: 626-34.

[7] Bai M and Bornhop DJ. Recent advances in receptor-targeted fluorescent probes for in vivo cancer imaging. Curr Med Chem 2012; 19: 4742-58.

[8] Boni L, David G, Mangano A, Dionigi G, Rausei S, Spampatti S, Cassinotti E and Fingerhut A. Clinical applications of indocyanine green (ICG) enhanced fluorescence in laparoscopic surgery. Surg Endosc 2014; [Epub ahead of print].

[9] Tu C, Ma X, Pantazis P, Kauzlarich SM and Louie AY. Paramagnetic, silicon quantum dots for magnetic resonance and two-photon imag-

ing of macrophages. J Am Chem Soc 2010; 132: 2016-23.

[10] Janjic JM, Shao P, Zhang S, Yang X, Patel SK and Bai M. Perfluorocarbon nanoemulsions with fluorescent, colloidal and magnetic properties. Biomaterials 2014; 35: 4958-68.

[11] Patel SK, Patrick MJ, Pollock JA and Janjic JM. Two-color fluorescent (near-infrared and visible) triphasic perfluorocarbon nanoemuslions. J Biomed Opt 2013; 18: 101312.

[12] Saxena A, Kessinger CW, Thompson B, McCarthy JR, Iwamoto Y, Lin CP and Jaffer FA. High-resolution optical mapping of inflammatory macrophages following endovascular arterial injury. Mol Imaging Biol 2013; 15: 282-9.

[13] Deguchi JO, Aikawa M, Tung CH, Aikawa E, Kim DE, Ntziachristos V, Weissleder R and Libby P. Inflammation in atherosclerosis: visualizing matrix metalloproteinase action in macrophages in vivo. Circulation 2006; 114: 55-62.

[14] Jaffer FA, Vinegoni C, John MC, Aikawa E, Gold HK, Finn AV, Ntziachristos V, Libby P and Weissleder R. Real-time catheter molecular sensing of inflammation in proteolytically active atherosclerosis. Circulation 2008; 118: 1802-9.

[15] Jaffer FA, Calfon MA, Rosenthal A, Mallas G, Razansky RN, Mauskapf A, Weissleder R, Libby P and Ntziachristos V. Two-dimensional intravascular near-infrared fluorescence molecular imaging of inflammation in atherosclerosis and stent-induced vascular injury. J Am Coll Cardiol 2011; 57: 2516-26.

[16] Kang NY, Park SJ, Ang XW, Samanta A, Driessen WH, Ntziachristos V, Vasquez KO, Peterson JD, Yun SW and Chang YT. A macrophage uptaking near-infrared chemical probe CDnir7 for in vivo imaging of inflammation. Chem Commun 2014; 50: 6589-91.

[17] Yoo JS, Das RK, Jow ZY and Chang YT. In vivo detection of macrophage recruitment in hindlimb ischemia using a targeted near-infrared fluorophore. PLoS One 2014; 9: e103721.

[18] Scotter EL, Abood ME and Glass M. The endocannabinoid system as a target for the treatment of neurodegenerative disease. Br J Pharmacol 2010; 160: 480-98.

[19] Klein TW, Newton C, Larsen K, Lu L, Perkins I, Nong L and Friedman H. The cannabinoid system and immune modulation. J Leukoc Biol 2003; 74: 486-96.

[20] Van Sickle MD, Duncan M, Kingsley PJ, Mouihate A, Urbani P, Mackie K, Stella N, Makriyannis A, Piomelli D, Davison JS, Marnett LJ, Di Marzo V, Pittman QJ, Patel KD and Sharkey KA. Identification and functional characterization of brainstem cannabinoid CB2 receptors. Science 2005; 310: 329-32.

[21] Leleu-Chavain N, Body-Malapel M, Spencer J, Chavatte P, Desreumaux P and Millet R. Recent

[22] advances in the development of selective CB(2) agonists as promising anti-inflammatory agents. Curr Med Chem 2012; 19: 3457-74.

[22] Zhang S, Shao P and Bai M. In vivo type 2 cannabinoid receptor-targeted tumor optical imaging using a near infrared fluorescent probe. Bioconjug Chem 2013; 24: 1907-16.

[23] Han Y. Ginkgo terpene component has an antiinflammatory effect on Candida albicans-caused arthritic inflammation. Int Immunopharmacol 2005; 5: 1049-56.

[24] Graham ES, Angel CE, Schwarcz LE, Dunbar PR and Glass M. Detailed characterisation of CB2 receptor protein expression in peripheral blood immune cells from healthy human volunteers using flow cytometry. Int J Immunopathol Pharmacol 2010; 23: 25-34.

[25] Moaddel R, Rosenberg A, Spelman K, Frazier J, Frazier C, Nocerino S, Brizzi A, Mugnaini C and Wainer IW. Development and characterization of immobilized cannabinoid receptor (CB1/CB2) open tubular column for on-line screening. Anal Biochem 2011; 412: 85-91.

[26] Fujiwara N and Kobayashi K. Macrophages in inflammation. Curr Drug Targets Inflamm Allergy 2005; 4: 281-6.

[27] Weissleder R, Nahrendorf M and Pittet MJ. Imaging macrophages with nanoparticles. Nat Mater 2014; 13: 125-38.

[28] Saleh A, Schroeter M, Jonkmanns C, Hartung HP, Modder U and Jander S. In vivo MRI of brain inflammation in human ischaemic stroke. Brain 2004; 127: 1670-7.

[29] Nahrendorf M, Zhang H, Hembrador S, Panizzi P, Sosnovik DE, Aikawa E, Libby P, Swirski FK and Weissleder R. Nanoparticle PET-CT imaging of macrophages in inflammatory atherosclerosis. Circulation 2008; 117: 379-87.

[30] Aikawa E, Nahrendorf M, Figueiredo JL, Swirski FK, Shtatland T, Kohler RH, Jaffer FA, Aikawa M and Weissleder R. Osteogenesis associates with inflammation in early-stage atherosclerosis evaluated by molecular imaging in vivo. Circulation 2007; 116: 2841-50.

[31] Longmire M, Choyke PL and Kobayashi H. Clearance properties of nano-sized particles and molecules as imaging agents: considerations and caveats. Nanomedicine 2008; 3: 703-17.

[32] Scotter EL, Abood ME and Glass M. The endocannabinoid system as a target for the treatment of neurodegenerative disease. Br J Pharmacol 2010; 160: 480-98.

[33] Galiegue S, Mary S, Marchand J, Dussossoy D, Carriere D, Carayon P, Bouaboula M, Shire D, Lefur G and Casellas P. Expression of central and peripheral cannabinoid receptors in human immune tissues and leukocyte subpopulations. Eur J Biochem 1995; 232: 54-61.

[34] Bai MF, Sexton M, Stella N and Bornhop DJ. MBC94, a conjugable ligand for cannabinoid

CB2 receptor imaging. Bioconjugate Chem 2008; 19: 988-92.

[35] Hsieh GC, Pai M, Chandran P, Hooker BA, Zhu CZ, Salyers AK, Wensink EJ, Zhan CC, Carroll WA, Dart MJ, Yao BB, Honore P and Meyer MD. Central and peripheral sites of action for CB2 receptor mediated analgesic activity in chronic inflammatory and neuropathic pain models in rats. Br J Pharmacol 2011; 162: 428-40.

[36] Maresz K, Carrier EJ, Ponomarev ED, Hillard CJ and Dittel BN. Modulation of the cannabinoid CB2 receptor in microglial cells in response to inflammatory stimuli. J Neurochem 2005; 95: 437-45.

[37] Evens N, Vandeputte C, Muccioli GG, Lambert DM, Baekelandt V, Verbruggen AM, Debyser Z, Van Laere K and Bormans GM. Synthesis, in vitro and in vivo evaluation of fluorine-18 labelled FE-GW405833 as a PET tracer for type 2 cannabinoid receptor imaging. Bioorg Med Chem 2011; 19: 4499-505.

[38] Horti AG, Gao Y, Ravert HT, Finley P, Valentine H, Wong DF, Endres CJ, Savonenko AV and Dannals RF. Synthesis and biodistribution of [11C]A-836339, a new potential radioligand for PET imaging of cannabinoid type 2 receptors (CB2). Bioorg Med Chem 2010; 18: 5202-7.

[39] Evens N, Vandeputte C, Coolen C, Janssen P, Sciot R, Baekelandt V, Verbruggen AM, Debyser Z, Van Laere K and Bormans GM. Preclinical evaluation of [11C]NE40, a type 2 cannabinoid receptor PET tracer. Nucl Med Biol 2012; 39: 389-99.

[40] Castaneda JT, Harui A, Kiertscher SM, Roth JD and Roth MD. Differential expression of intracellular and extracellular CB(2) cannabinoid receptor protein by human peripheral blood leukocytes. J Neuroimmune Pharmacol 2013; 8: 323-32.

[41] Yates AS, Doughty SW, Kendall DA and Kellam B. Chemical modification of the naphthoyl 3-position of JWH-015: In search of a fluorescent probe to the cannabinoid CB2 receptor. Bioorg Med Chem Lett 2005; 15: 3758-62.